Available online at www.sciencedirect.com
ScienceDirect
Computers and Structures 86 (2008) 1633–1642
Computers & Structures
www.elsevier.com/locate/compstruc

A study of suspended roofs for near-source seismic motions

Ioannis G. Raftoyiannis *, Constantine C. Spyrakos

Department of Civil Engineering, National Technical University of Athens, 9 Iroon Polytechneiou Str., Zografou Campus, Athens 15780, Greece

Received 18 December 2006; accepted 16 January 2008
Available online 7 March 2008

Abstract

The non-linear behavior of multi-suspended roof systems for seismic loads is studied. The study is based on a formulation that can be easily employed for a preliminary design of multi-suspended roofs subjected to seismic loads. Specifically, applying Lagrange's equations, the corresponding set of equations of motion for discrete models of multiple suspension roofs is obtained and numerical integration of the equations of motion is performed via the Runge–Kutta scheme. For representative realistic combinations of geometric, stiffness and damping parameters, a non-linear analysis is employed to study the behavior of suspended roofs for near-source and far-field seismic motions. The analysis demonstrates that: (i) code-specified design loads could dramatically underestimate the response of suspended roofs subjected to near-source ground motions and (ii) flexible roofing systems are greatly affected by near-source ground motions, a behavior that is not observed for stiff systems.

Keywords: Multiple suspension roofs; Non-linear analysis; Seismic response; Near-source motions

1. Introduction

Many modern structural buildings, such as commercial halls, airport halls, sport centers, trade and exhibition centers utilize suspension roofs that combine stability, economy and satisfaction of special architectural demands. A number of inspired engineers have designed and built numerous great buildings with suspended roofs as their main structural component [1–3].

In the last two decades, the development of powerful computers and sophisticated non-linear FEM software has enabled engineers to utilize suspension roofs in complicated large-scale structures, some of which can be classified among unique examples of engineering excellence [4,5].

The current state of practice for non-linear static and dynamic stability analysis of suspended structures, including suspension roof systems, can be achieved through sophisticated FEM programs, which can simulate the actual structures with models containing a large number of degrees of freedom [6]. Nevertheless, modelling of suspension roof systems with finite elements for design purposes is a time consuming procedure that requires special experience. On the other hand, simplified models for suspension roof systems with a few degrees-of-freedom could simulate the response of real continuous structures, provided that these models embrace the salient features of the structural behavior [7,8].

Suspended roof systems used world-wide require three-dimensional suspensions and transverse stiffening, being sensitive to horizontal vibrations and may lose their stability due to dynamic snap-through buckling [9,10]. On the other hand, double and multiple suspension roofs may overcome the aforementioned disadvantages of single suspensions with repeated plane configurations [11], which can effectively resist uplift and unbalanced as well as upward and downward loading, as illustrated schematically in Fig. 1.

Abbreviations: EAK, Greek Seismic Code; EC, Eurocode.

* Corresponding author. Tel.: +30 210 7722454; fax: +30 210 7722482.
E-mail address: rafto@central.ntua.gr (I.G. Raftoyiannis).

0045-7949/$ - see front matter © 2008 Elsevier Ltd. All rights reserved.
doi:10.1016/j.compstruc.2008.01.005

As flexible systems, the response of suspended roofs is mostly affected by dynamic loads characterized by long periods [9]. The response of such systems to wind loads has been extensively studied [10,5] and is currently addressed in several codes, e.g., Eurocode 1 [12]. The long eigenperiods that characterize these systems can safeguard them from seismic motions that are characterized by short period ground reversals; however, they can be an issue of concern for near-source ground motions characterized by long duration pulses.

Studies on the response of structures located at near-source has been substantially increased after the 1994 Northridge earthquake and the more recent 1995 Kobe earthquake [13,14]. The ground motion parameters of the 1994 Northridge earthquake have far reaching implications in seismic design and especially on the design of flexible structures. It has been reported that structures in the middle period range (natural periods of 0.5–2.5 s) appear to be mostly affected from motions characterized by a ground velocity pulse, while large ground displacement pulses are damaging to long period structures, i.e., natural periods longer than 3 s [15–18]. However, one should acknowledge the pioneering work of other investigators such as Bertero et al. [19], who studied the response of structures to the near-source motion of the San Fernando earthquake.

The high-energy pulses of motion encountered at sites affected by forward directivity, often referred as "fling" [20] result in exceptionally high spectral response ordinates, particular at longer periods. The phenomenon is primarily attributed to distinctive pulse-like time histories, high peak velocities and large ground displacements exhibited especially on the fault-normal component [17], a fact that is recognized and accounted for by current seismic codes and provisions, e.g., NEHRP [21], IBC [22] and EAK [23]. Specifically, the UBC 97, the first seismic design code [24] that explicitly introduced specific procedures to account for near-source effects through the application of spectral amplification factors, implies that for earthquakes of M 7 and greater, the near field is limited to 15 km from the fault and that the near-filed does not exist for earthquakes smaller than M 6.5. Recent studies, however, considering as near-source the area close to the earthquake source where ground motions are sufficiently strong to induce damage in engineered structures, have shown that near-source effects should be considered for all earthquakes regardless of magnitude to a lower limit as M 4.5 [25]. For earthquakes of less than M 6.5 near-source pulses appear at shorter periods of the order of 0.5 s [26–28]. Salient differences between "near" and "far" field records as well as their effects on structures have been studied by several researchers [29–31].

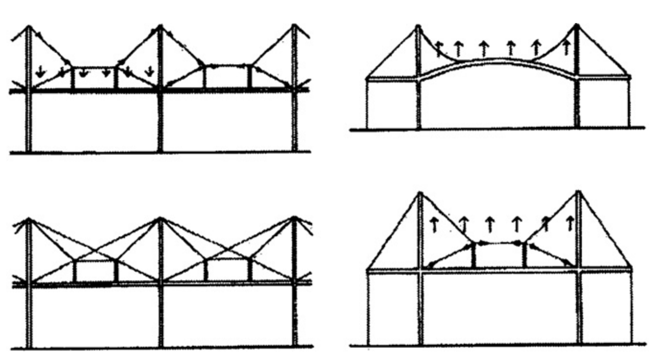

Fig. 1. Simple models for suspension roofing systems.

Near-source ground motions with pulses can induce dramatically high responses that could far exceed the capacity of flexible structures [32]. Iwan [33] stated that the pulses in near-source ground motions travel through the height of the buildings as waves, and that the conventional techniques using the modal superposition method and the response spectrum analysis may not capture the effects of these pulses.

The primary objective of this study is twofold: (i) to formulate the problem of seismic analysis of suspended roofs with a methodology that can be easily implemented to preliminary design and (ii) to investigate the response of suspended roofs to near-source ground motions. To the author's knowledge this is the first study of its own on the seismic response of suspended roofing systems to near-source seismic motions. Based on energy principles, the equations of the system are formulated in a non-dimensional form in order to facilitate parametric analysis, and numerically solved with a Runge–Kutta scheme.

2. Equations of motion

Usually suspended roofing systems are mounted on elastic supports and consist of a space truss with hinged connected parts and a number of suspension bars holding the system at the supports. In this study the N-DOF system shown in Fig. 2 is used as a simple, yet realistic, simulation of multi-suspension roofs [8]. The model consists of $N-1$ vertical linear springs with stiffness k_i $(i=2,3,\ldots,N)$, corresponding dashpots c_i $(i=2,3,\ldots,\mathrm{N})$ and $N-1$ concentrated masses m_i $(i=2,3,\ldots,N)$ interconnected via $N-2$ weightless rigid inextensional bars of length ℓ_i. In Fig. 2 the dampers are not shown for simplicity. The nodal supports 1 and $N+1$ are immovable hinges connected with the masses m_2 and m_N through inclined springs with stiffness k_1 and k_{N+1}, and dashpots c_1 and c_{N+1}, respectively. The elastic supports are modelled with the springs k_1 and k_{N+1} considered as extensional bars with initial length $\ell_{1,0}$ and $\ell_{N,0}$, respectively, while in the deformed state (shown with dotted lines in Fig. 2) their length becomes ℓ_1 and ℓ_N, respectively. Since the suspension springs 2–N are acting mainly in the vertical direction and the system is anticipated to experience reasonably small horizontal deflections compared to the total length of the system, it can be assumed that the supports of the vertical springs can freely slide along horizontal tracks as shown in Fig. 2.

The initial configuration of the system can be described by the bar lengths $\ell_{1,0},\ell_2,\ldots,\ell_{N-1}$ and $\ell_{N,0}$, and the corresponding direction angles $\theta_{1,0},\theta_{2,0},\ldots,\theta_{N-1,0}$ and $\theta_{N,0}$.

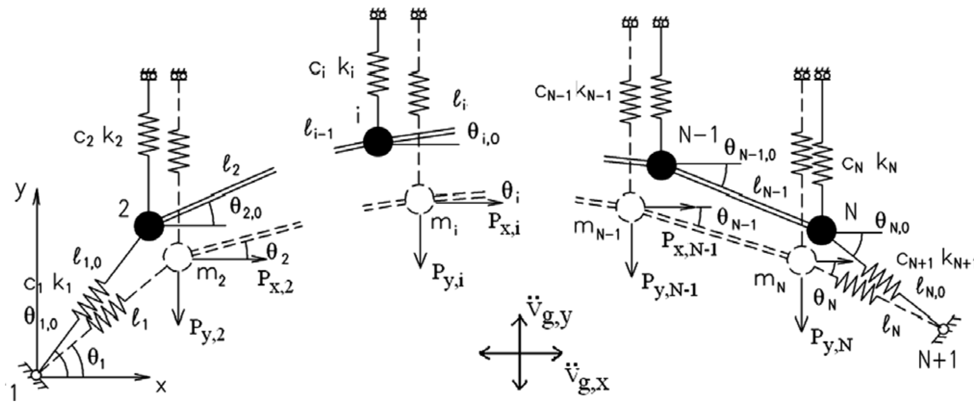

Fig. 2. N-DOF system for a multiple suspension roof.

Since nodes 1 and $N+1$ are immovable hinges, the deformed configuration is described by the bar length ℓ_1 and the angles $\theta_1, \theta_2, \ldots, \theta_{N-1}$. The system is initially at rest in a configuration described by the following set of equations:

$$\left.\begin{aligned} x_{i,0} &= \ell_{1,0}\cos\theta_{1,0} + \sum_{j=2}^{i}\ell_j\cos\theta_{j,0} \\ y_{i,0} &= \ell_{1,0}\sin\theta_{1,0} + \sum_{j=2}^{i}\ell_j\sin\theta_{j,0} \end{aligned}\right\} \tag{1}$$

where $x_{i,0}$ and $y_{i,0}$ are the initial coordinates of joint i, and ℓ_j and $\theta_{j,0}$ are the length and the initial direction angle of bar j, respectively. The deformed configuration of the system is described by

$$\left.\begin{aligned} x_i &= \ell_1\cos\theta_1 + \sum_{j=2}^{i}\ell_j\cos\theta_j \\ y_i &= \ell_1\sin\theta_1 + \sum_{j=2}^{i}\ell_j\sin\theta_j \end{aligned}\right\} \tag{2}$$

where x_i and y_i are the coordinates of joint i, and θ_j is the direction of bar j in the deformed position. The strain energy U of the system can be expressed as [34]

$$\begin{aligned} U = {} & \frac{1}{2}k_1(\ell_1-\ell_{1,0})^2 + \frac{1}{2}\sum_{i=2}^{N}k_i\left(\ell_1\sin\theta_1 + \sum_{j=2}^{i-1}\ell_j\sin\theta_j \right. \\ & \left. - \ell_{1,0}\sin\theta_{1,0} - \sum_{j=2}^{i-1}\ell_j\sin\theta_{j,0}\right)^2 \\ & + \frac{1}{2}k_{N+1}\left\{\left[\left(\ell_{1,0}\cos\theta_{1,0} + \sum_{j=2}^{N-1}\ell_j\cos\theta_{j,0} + \ell_{N,0}\cos\theta_{N,0}\right.\right.\right. \\ & \left. - \sum_{j=1}^{N-1}\ell_j\cos\theta_j\right)^2 + \left(\ell_{1,0}\sin\theta_{1,0} + \sum_{j=2}^{N-1}\ell_j\sin\theta_{j,0}\right. \\ & \left.\left.\left. + \ell_{N,0}\sin\theta_{N,0} - \sum_{j=1}^{N-1}\ell_j\sin\theta_j\right)^2\right]^{\frac{1}{2}} - \ell_{N,0}\right\} \end{aligned} \tag{3}$$

Since the system is modelled with concentrated masses m_i while ignoring the rotational inertia of the rigid links, the load potential Ω due to the earthquake loads $P_i(t)$ applied at the joints in the form of horizontal and vertical components, i.e., $P_{x,i}(t)$ and $P_{y,i}(t)$, is given by

$$\begin{aligned} \Omega = {} & -\sum_{i=2}^{N}P_{x,i}(t)\left[\ell_1\cos\theta_1 + \sum_{j=2}^{i-1}\ell_j\cos\theta_j - \ell_{1,0}\cos\theta_{1,0}\right. \\ & \left. - \sum_{j=2}^{i-1}\ell_j\cos\theta_{j,0}\right] - \sum_{i=2}^{N}P_{y,i}(t)\left[\ell_1\sin\theta_1 + \sum_{j=2}^{i-1}\ell_j\sin\theta_j\right. \\ & \left. - \ell_{1,0}\sin\theta_{1,0} - \sum_{j=2}^{i-1}\ell_j\sin\theta_{j,0}\right] \end{aligned} \tag{4}$$

The kinetic energy K of the system is

$$\begin{aligned} K = {} & \frac{1}{2}\sum_{i=2}^{N}m_i\left[\left(\dot{\ell}_1\cos\theta_1 - \ell_1\dot{\theta}_1\sin\theta_1 - \sum_{j=2}^{i-1}\ell_j\dot{\theta}_j\sin\theta_j\right)^2\right. \\ & \left. + \left(\dot{\ell}_1\sin\theta_1 + \ell_1\dot{\theta}_1\cos\theta_1 + \sum_{j=2}^{i-1}\ell_j\dot{\theta}_j\cos\theta_j\right)^2\right] \end{aligned} \tag{5}$$

and the dissipation energy F is

$$\begin{aligned} F = {} & \frac{1}{2}c_1\left(\dot{\ell}_1^2 + \ell_1^2\dot{\theta}_1^2\right) + \frac{1}{2}\sum_{i=2}^{N}c_i\left(\dot{\ell}_1\sin\theta_1 + \sum_{j=1}^{i-1}\ell_j\dot{\theta}_j\cos\theta_j\right)^2 \\ & + \frac{1}{2}c_{N+1}\left[\left(\dot{\ell}_1\cos\theta_1 - \sum_{j=1}^{N-1}\ell_j\dot{\theta}_j\sin\theta_j\right)^2\right. \\ & \left. + \left(\dot{\ell}_1\sin\theta_1 + \sum_{j=1}^{N-1}\ell_j\dot{\theta}_j\cos\theta_j\right)^2\right] \end{aligned} \tag{6}$$

The Lagrange equations of motion of the system are expressed by

$$\left.\begin{array}{l}\frac{\partial}{\partial t}\left(\frac{\partial K}{\partial \dot{\ell}_1}\right)-\frac{\partial K}{\partial \ell_1}+\frac{\partial F}{\partial \dot{\ell}_1}+\frac{\partial U}{\partial \ell_1}=-\frac{\partial \Omega}{\partial \ell_1}\\ \frac{\partial}{\partial t}\left(\frac{\partial K}{\partial \dot{\theta}_1}\right)-\frac{\partial K}{\partial \theta_1}+\frac{\partial F}{\partial \dot{\theta}_1}+\frac{\partial U}{\partial \theta_1}=-\frac{\partial \Omega}{\partial \theta_1}\\ \cdots\\ \frac{\partial}{\partial t}\left(\frac{\partial K}{\partial \dot{\theta}_{N-1}}\right)-\frac{\partial K}{\partial \theta_{N-1}}+\frac{\partial F}{\partial \dot{\theta}_{N-1}}+\frac{\partial U}{\partial \theta_{N-1}}=-\frac{\partial \Omega}{\partial \theta_{N-1}}\end{array}\right\} \quad (7)$$

The system shown in Fig. 2 is considered initially imperfect, which implies that some joints have undergone a small initial deformation for which all springs are considered to be unstressed. In order to facilitate the parametric study that follows, non-dimensional quantities are introduced into Eq. (7)

$$\left.\begin{array}{l}\lambda=\frac{P_2}{k_1\ell_{1,0}},\quad \tau=\sqrt{\frac{k_1}{m_2}}t,\quad \bar{\ell}_{N,0}=\ell_{N,0}/\ell_{1,0}\\ \bar{m}_i=m_i/m_2,\quad p_i=P_i/P_2,\quad \bar{\ell}_i=\ell_i/\ell_{1,0}\ \ (i=2,\ldots,N)\\ \bar{c}_i=c_i/\sqrt{k_1m_2},\quad \bar{k}_i=k_i/k_1\end{array}\right\} \quad (8)$$

where k_1 and $\ell_{1,0}$ are the stiffness and the initial length of the spring at the left support, respectively, and m_2 and P_2 are the mass and total magnitude of seismic force at node 2, respectively. After manipulation of the resulting expressions, the equations of motion are numerically solved in a non-dimensional form. Numerical difficulties, caused by strong non-linearities associated with convergence failure have been faced in the process of solving Eq. (7) via the Runge–Kutta scheme. This problem has been efficiently treated by decreasing the size of the relevant integration step [35], with negligible effect on the accuracy of the results, as elaborated in the following section.

3. Numerical examples

The numerical examples refer to the triply suspended roof model (4-DOF system) shown in Fig. 3 with $\bar{\ell}_2=\bar{\ell}_3=3$, $\bar{\ell}_{4,0}=1$, $2\bar{m}_3=\bar{m}_4=0.5$, $\theta_{2,0}=-\theta_{3,0}=30°$ and $\theta_{1,0}=-\theta_{4,0}=45°$. For representative geometrical configurations and a wide range of mechanical properties, the dynamic response of each system is obtained for several types of seismic excitations. The following representative cases have been studied by varying the suspension stiffness (k_2,k_3,k_4) with reference to the lateral support stiffness

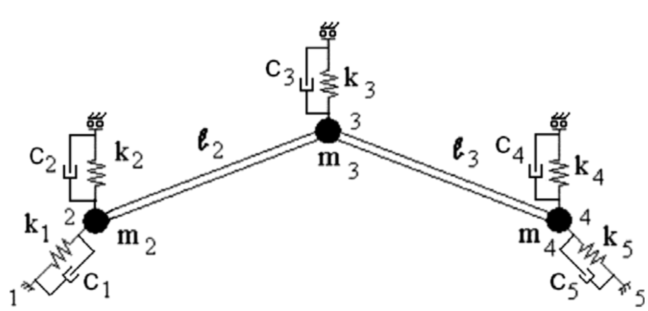

Fig. 3. Triple suspension roof model.

(k_1=k_5): (i) stiff suspension ($\bar{k}_2=2\bar{k}_3=\bar{k}_4=1$), (ii) medium suspension ($\bar{k}_2=2\bar{k}_3=\bar{k}_4=0.5$), and (iii) flexible suspension systems ($\bar{k}_2=2\bar{k}_3=\bar{k}_4=0.1$). In all cases, the suspension and the lateral support damping coefficients are evaluated for a damping ratio $\xi=2\%$. Thus, in view of Eq. (8), the corresponding non-dimensional dashpot coefficients are $\bar{c}_1=\bar{c}_2=\bar{c}_3=\bar{c}_4=0.028$.

Table 1 presents the first three eigenperiods of the triple suspension roof model that correspond to horizontal, vertical and coupled modes, respectively. It is observed that the period associated with the horizontal mode is the least affected by the variation of the suspension stiffness, in contrast to the other two periods that dominate the vertical motion.

The system of the four second-order non-linear equations of motion, Eq. (7), is given a small initial deformation with $\theta^*_{2,0}=0.5°$ and treated numerically as a system of eight first-order ordinary differential equations via the Runge–Kutta scheme yielding a minimal error $O(h^4)$, with h denoting the integration step [35]. It has been found that for a step size $h<0.001$, the numerical integration procedure is stable for all cases. The system response has been obtained via the Mathematica software [36], for representative suspension stiffness, near-source seismic records and artificial accelerograms, as discussed in the following.

In order to investigate the behavior of the system to near-source ground motions and examine the adequacy of seismic codes to account for near-source motions, a set of records of near-source motions recorded on rock and soft sites has been selected. Table 2 lists characteristics of the selected earthquakes. Ground accelerations from the 06-15-1995 Aegion earthquake and the 08-19-2003 Lefkas earthquake recorded a few kilometres from the epicentres have been chosen. The horizontal near-source acceleration records of the Aegion and Lefkas events are characterized by acceleration pulses with a maximum amplitude of 0.52 g as shown in Fig. 4a and b, respectively. The velocity traces of the events contain two distinct pulses with a duration of 0.6–0.7 s and amplitude of about 44 cm/s [37]. For reasons of comparison, the system is also subjected to artificial earthquakes corresponding to the Greek Aseismic Code – EAK [23] response spectra for soil category B (strongly weathered rocks and layers of granular material with medium density) and the maximum ground accelerations 0.24 g and 0.36 g shown in Fig. 5a and b, respectively. The artificial earthquakes have been generated to correspond to the Aegion and Lefkas records, respectively.

Table 1
Natural periods of the 4-DOF roof model for various stiffness parameters

	$\bar{k}_2=2\bar{k}_3=\bar{k}_4=1$	$\bar{k}_2=2\bar{k}_3=\bar{k}_4=0.5$	$\bar{k}_2=2\bar{k}_3=\bar{k}_4=0.1$
T_1 (s)	1.967 (v)	1.669 (v)	1.323 (v)
T_2 (s)	1.528 (c)	1.179 (c)	1.125 (h)
T_3 (s)	0.926 (h)	0.914 (h)	0.710 (c)

Note: (h) horizontal mode, (v) vertical mode and (c) coupled vertical and rotational mode.

Table 2
Strong motion data set of earthquake records

No	Earthquake	Date	Fault mechanism	Magnitude (M_w)	Station	Component	PGA (g)	PGV (cm/s)	PGD (cm)	Distance (km)	SI_V (cm/s)
1	Lefkas	11/04/1973	RN	5.8	OTE building	L	0.50	45.15	4.4S	R_{hyp} 23.0	168
2	Aeaion	06/15/1955	N	6.4	OTE building	T	0.52	43.01	4.53	R_{hyp} 21.0	147
3	Northridge	01/17/1994	RN	6.7	Sylniar, CA – County Hospital	90	0.604	76.9	20.2	R_{epi} 15.8	259
4	Loma Prieta	10/18/1989	RO	7.0	Hollister, CA – South Street and Pine Drive	0	0.370	62.2	31.9	R_{epi} 50.0	252
5	Morgan Hill	04/24/1984	SS	6.1	Gilroy Array #6	90	0.286	36.6	5.2	R_{epi} 36.0	150
6	Coalinga	05/02/1983	RO	6.4	Pleasant Valley, CA – Pumping Plant	135	0.524	39.1	6.6	R_{epi} 9.0	156

RN: reverse fault, RO: reverse-oblique fault, SS: strike slip fault, N: normal fault, R_{hyp}: hypocentral, R_{epi}: epicentral, R_{wp}: closest to fault rupture and SI_V, velocity spectrum intensity.

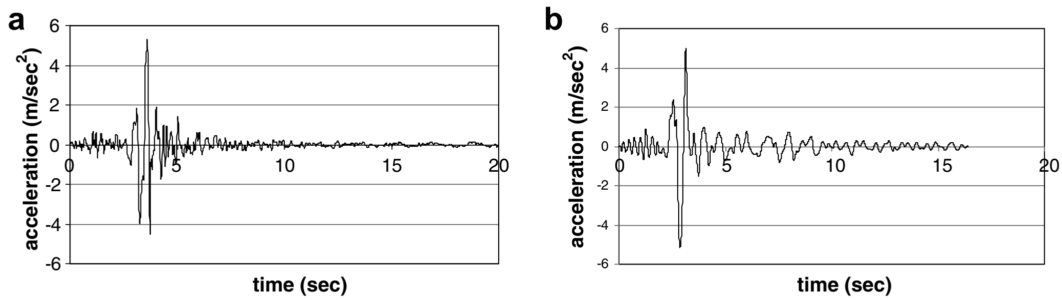

Fig. 4. Aegion (a) and Lefkas (b) accelerograms, respectively.

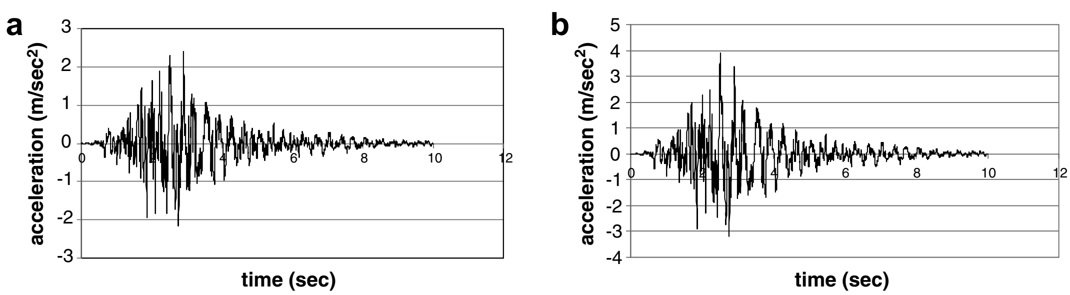

Fig. 5. Artificial accelerograms EAK with $A_g = 0.24$ g (a), and $A_g = 0.36$ g (b), respectively.

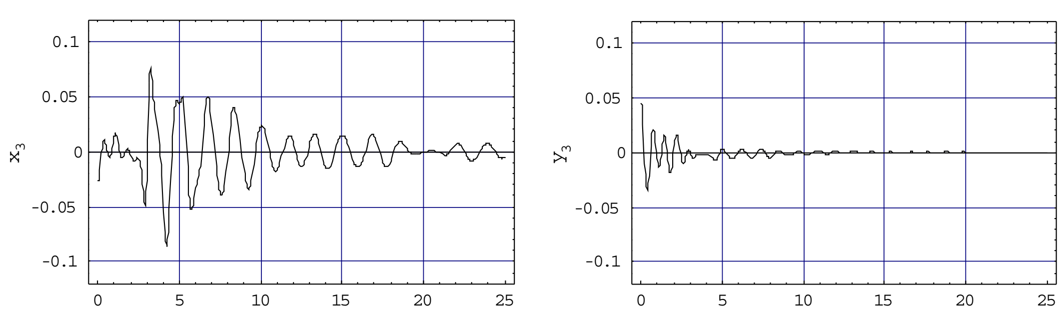

Fig. 6. Response of the 4-DOF model with $\bar{k}_2 = \bar{k}_3 = 1$ for the Aegion earthquake.

In Figs. 6–9, x_3 and y_3 denote the horizontal and vertical response of the central node 3, respectively. Figs. 6 and 7 show the responses for stiff and soft triple suspension models, respectively, subjected to the Aegion earthquake. Figs. 8 and 9 present the response for the same models for the Lefkas earthquake. From these figures it can be observed

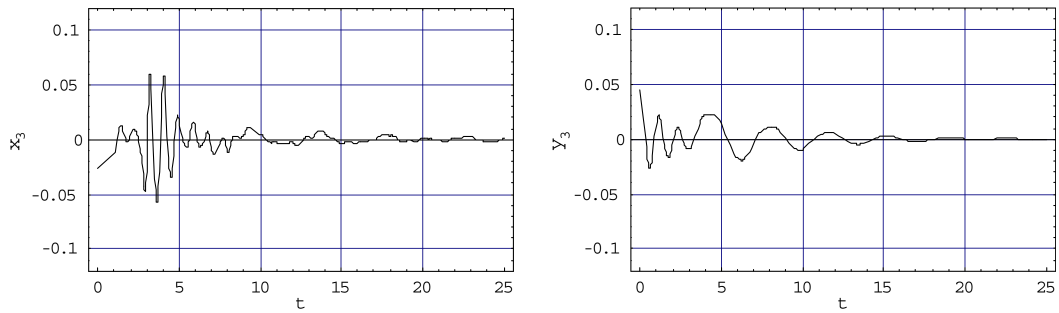

Fig. 7. Response of the 4-DOF model with $\bar{k}_2 = \bar{k}_3 = 0.1$ for the Aegion earthquake.

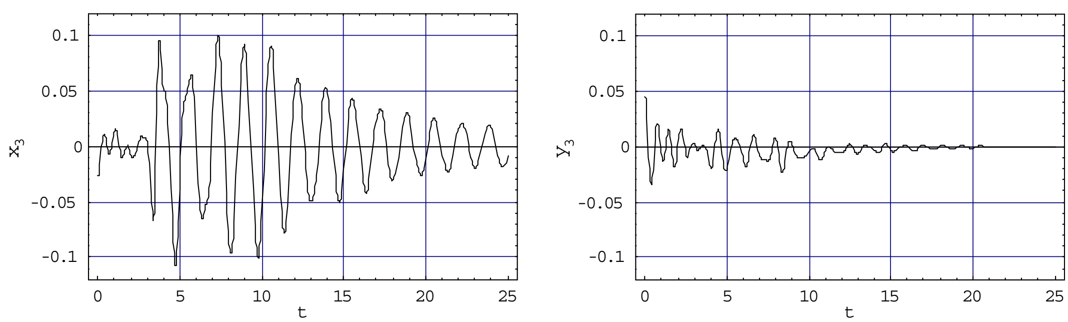

Fig. 8. Response of the 4-DOF model with $\bar{k}_2 = \bar{k}_3 = 1$ for the Lefkas earthquake.

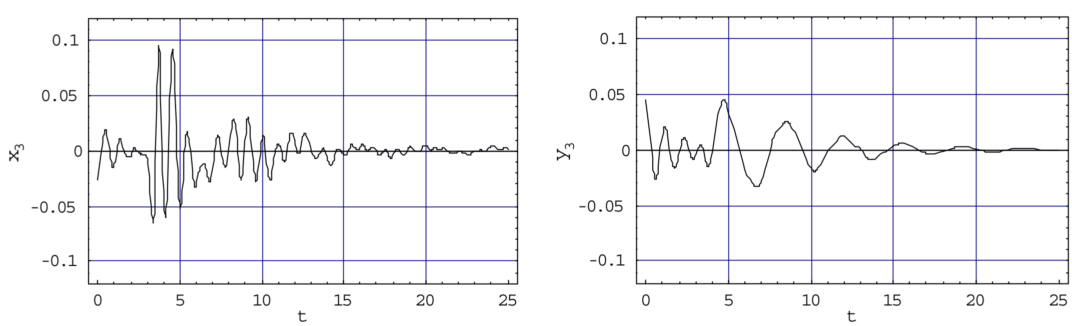

Fig. 9. Response of the 4-DOF model with $\bar{k}_2 = \bar{k}_3 = 0.1$ for the Lefkas earthquake.

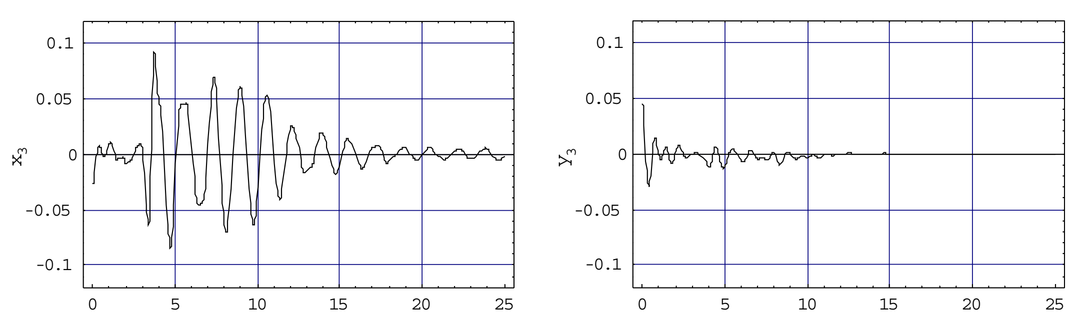

Fig. 10. Response of the 4-DOF model with $\bar{k}_2 = \bar{k}_3 = 1$ for the Lefkas earthquake ($\xi = 15\%$).

that: (a) as the suspension stiffness increases the duration of strong system response is elongated and (b) as the suspension stiffness decreases the system experiences substantially larger amplitudes in the vertical direction. More specifically, a decrease of 15–20% of the amplitude is observed in the horizontal direction, while an increase of 50–90% occurs in the vertical direction.

Fig. 10 shows the response of a 4-DOF roof with strong suspension and a damping ratio $\xi = 15\%$ for the Lefkas earthquake. This figure demonstrates the significant effect of damping in reducing the system response by about 50% in both the vertical and the horizontal direction. A similar behavior is observed for the effect of damping for the other stiffnesses and seismic records, a fact that can be used in order to significantly reduce the response of roofing systems to near-source ground motions.

Figs. 11 and 12 show the response of the stiff and soft suspension systems for the artificial earthquake generated from the EAK spectra, that corresponds to the Aegion record. It is observed that the response of the roof for the Aegion earthquake exceeds by about 20% the response of the artificial earthquake for the stiff suspension and by 15% for the soft suspension systems. A similar behavior is observed for the artificial record corresponding to the Lefkas earthquake as shown in Figs. 13 and 14.

In order to compare the response of suspended roofs when excited by near-source motions and records obtained at greater distances from the fault, the following two different pairs of records are selected:

(i) the first pair consists of a record for the Loma Prieta 18-10-1989 earthquake ($M_w = 7.0$) obtained at the Hollister – South Street and Pine Drive station at a 50 km epicentral distance, and a record for the Northridge 17-01-1994 earthquake ($M_w = 6.7$) obtained at the Sylmar, CA – County Hospital station at a 15.8 km epicentral distance,

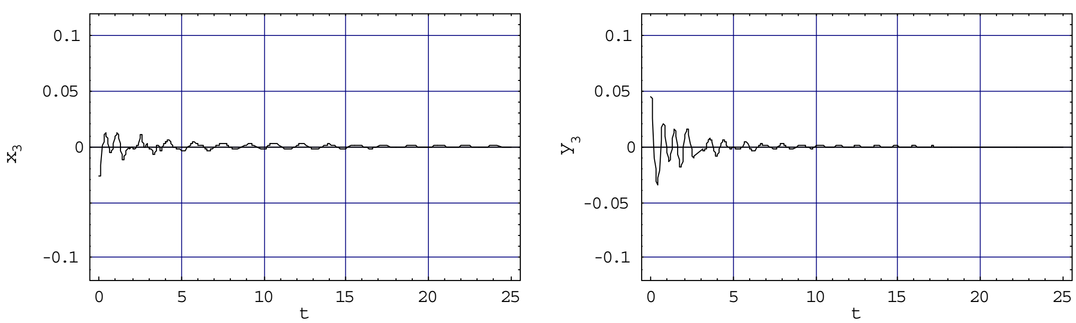

Fig. 11. Response of the 4-DOF model with $\bar{k}_2 = \bar{k}_3 = 1$ for EAK (0.24 g).

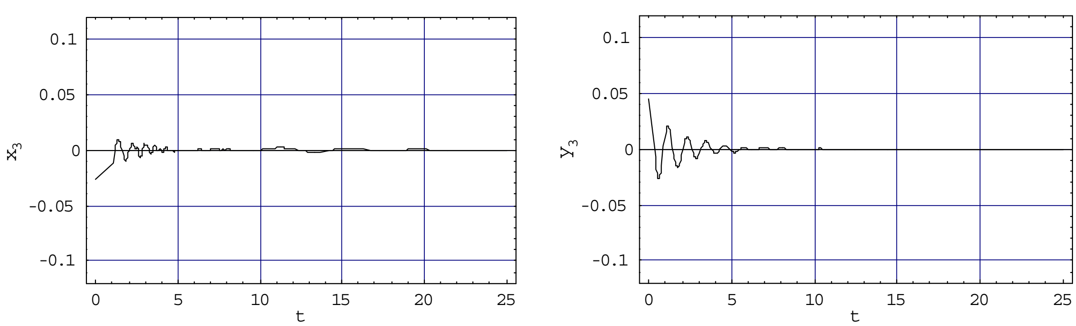

Fig. 12. Response of the 4-DOF model with $\bar{k}_2 = \bar{k}_3 = 0.1$ for EAK (0.24 g).

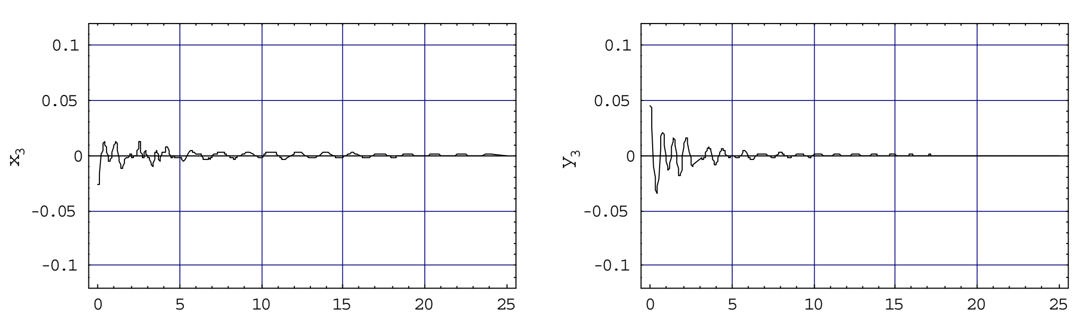

Fig. 13. Response of the 4-DOF model with $\bar{k}_2 = \bar{k}_3 = 1$ for EAK (0.36 g).

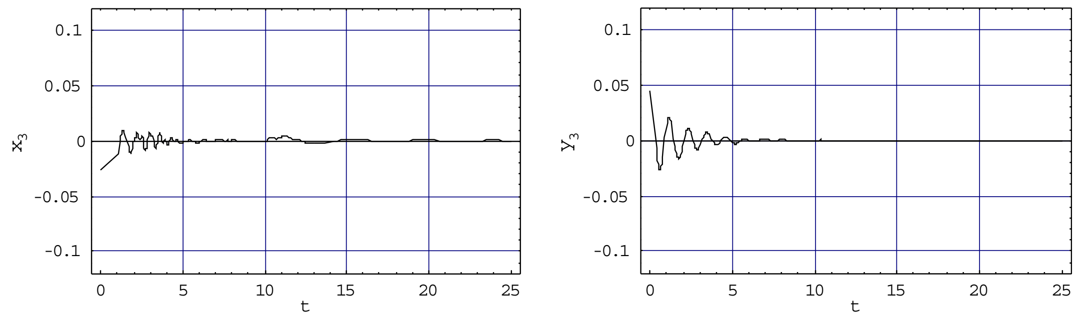

Fig. 14. Response of the 4-DOF model with $\bar{k}_2 = \bar{k}_3 = 0.1$ for EAK (0.36 g).

(ii) the second pair consists of a record for the Morgan Hill 24-04-1984 earthquake ($M_w = 6.1$) obtained at the Gilroy Array #6 station at 36 km epicentral distance, and a record for the Coalinga 02-05-1983 earthquake ($M_w = 6.4$) obtained at the Pleasant Valley, CA – Pumping Plant station at 9 km epicentral distance [38,39]. The accelerograms have been selected in order to have nearly the same velocity spectrum intensity (SI_V), a parameter that has been found to give the least scatter and the best fit to a target spectrum over the entire range of periods when scaling earthquake records for engineering analysis [40]. The SI_V parameter is given by the expression

$$SI_V = \int_{0.1}^{2.5} S_V(\xi, T)\mathrm{d}T \tag{9}$$

where S_V is the elastic pseudo-velocity spectrum and T is the response period. A damping ratio $\xi = 0.05$ has been selected for the analysis. Detailed characteristics of the records are presented in Table 2. The records of the Loma Prieta and the Morgan Hill earthquakes are characterized by a single prominent velocity pulse, while the records of the Northridge and the Coalinga earthquakes have more than one number of cycles of motion in their velocity traces [38,39]. The responses of the stiff suspension and soft suspension systems for the Northridge earthquake are shown in Figs. 15 and 16, respectively. Figs. 17 and 18 depict the responses of the same systems for the Loma Prieta earthquake, respectively.

Regarding the pair of the Northridge and the Loma Prieta earthquakes for stiff roofing systems, Figs. 15–18 show that as the stiffness decreases, the amplitude in the horizontal direction, x_3, decreases by 30–50%. For the pair of the Coalinga and the Morgan Hill earthquakes, the results (not shown herein for reasons of space saving) depict that

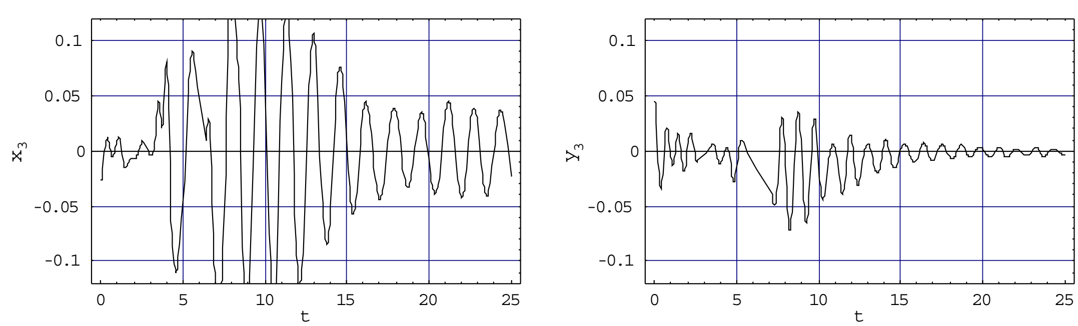

Fig. 15. Response of 4-DOF model with $\bar{k}_2 = \bar{k}_3 = 1$ for the Northridge earthquake.

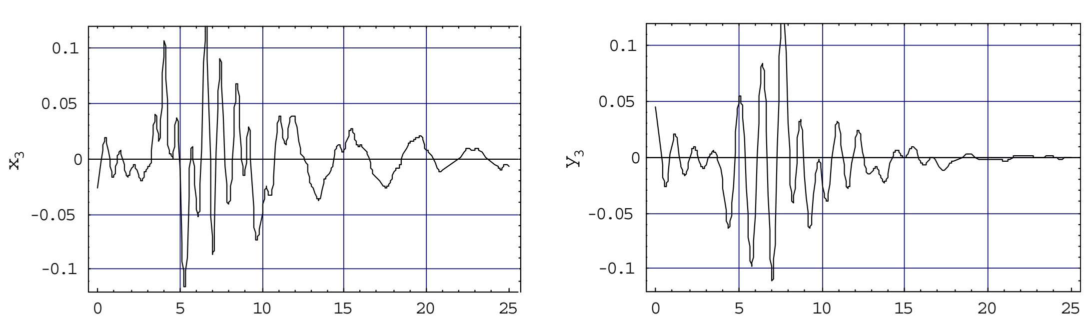

Fig. 16. Response of 4-DOF model with $\bar{k}_2 = \bar{k}_3 = 0.1$ for the Northridge earthquake.

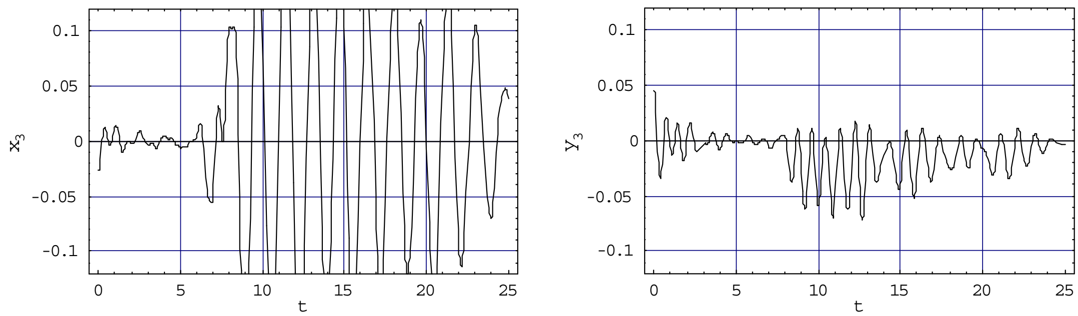

Fig. 17. Response of 4-DOF model with $\bar{k}_2 = \bar{k}_3 = 1$ for the Loma Prieta earthquake.

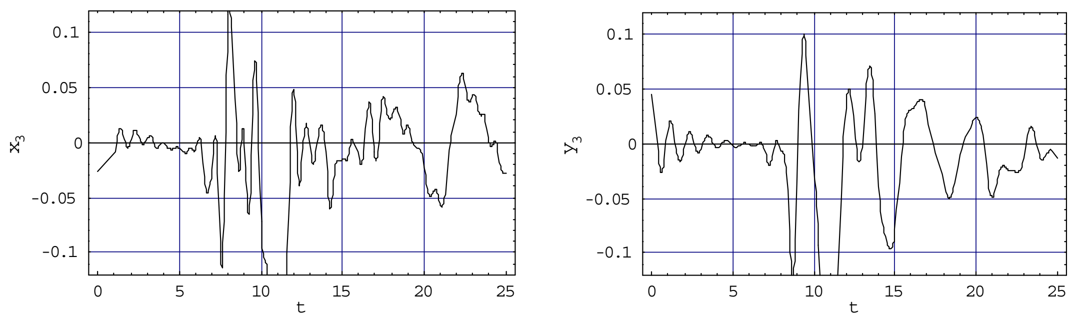

Fig. 18. Response of 4-DOF model with $\bar{k}_2 = \bar{k}_3 = 0.1$ for the Loma Prieta earthquake.

as the stiffness decreases, the amplitude in the horizontal direction, x_3, decreases by almost 50%. Regarding the vertical direction, y_3, of stiff systems for the far-field and near-source motions of the Northridge and the Loma Prieta earthquakes, small differences on the responses are observed in Figs. 15–18. This behavior indicates that differences between far-field and near-source ground motions do not affect the vertical response of stiff roofing systems. However, as Figs. 15 and 17 demonstrate, there are significant differences in the order of 300–400% regarding the vertical response of soft roofing systems. This behavior clearly demonstrates that flexible roofing systems are greatly affected from the pulses characterizing near-source records, a fact that requires proper attention for the seismic design of suspended roofs. Parametric studies, that are not shown herein, indicate intermediate differences on the vertical response for roofs with medium suspension stiffness.

4. Conclusions

This study presents a methodology to determine the response of multi-suspended roofing systems for seismic loads. It proposes a multi-DOF model that can serve as a means to consider the main dynamic characteristics of multiple suspension roofs and offer an insight on the advantages of this popular roofing system. In addition, it can be readily employed for preliminary design and assessment of the global stability of multi-suspended roof systems under seismic loads.

Since flexible systems are more vulnerable to near-source seismic motions characterized by ground response pulses, the study focuses on a parametric evaluation and assessment of the response of roofing systems for selected near-source seismic records. It also examines the sufficiency of current seismic codes, such as the Greek Aseismic Code (EAK 2000) to design suspended roofs for near-source seismic motions. The most important conclusions of this study can be summarised as follows:

– For all cases that are examined in this study, the response the system is stable (bounded motion), a primary advantage of multi-suspension roofs that is successfully captured by the proposed methodology.
– The vertical stiffness of the suspension system dominates the response of the roof, while the effect of the lateral support stiffness is less important.
– As the suspension stiffness increases the duration of the vertical response is elongated, while for decreasing suspension stiffness, the system experiences larger amplitudes in the vertical direction.
– The effect of damping is very significant for drastic reduction of the system response.
– The Greek Aseismic Code – EAK can significantly underestimate the response of suspension roofs.
– A comparison between the responses of flexible roofing systems for far-field and near-source records shows that the response of such systems is greatly affected in the vertical direction from pulses characterizing near-source records, while substantially smaller differences are observed for amplitudes in the horizontal direction.

In conclusion, this study demonstrates the fact that flexible roofing systems should be properly designed for sites in the vicinity of active faults. Further studies based on similar "pair" seismic records will enhance our understanding regarding the differences between the response of flexible roofing systems to far-field and near-source seismic records.

References

[1] Otto F. Das hangende Dach. Berlin: Bauwelt Verlag; 1954.
[2] Rabinovich L. Hangerdacher. Wiesbaden: Bauverlag Gmbh; 1962.
[3] Nervi PL. New structures. London: The Architectural Press; 1963.
[4] Kultermann U, Kenzo T. Works and projects. Barcelona: G. Gilli; 1989.
[5] Szabo J, Kollar L. Structural design of cable-suspended roofs. Chichester, UK: Ellis Norwood; 1984.
[6] Wagner R. Cable and membrane structures. Berlin: Ernst & Sohn; 2002.
[7] Sophianopoulos DS, Michaltsos GT. Nonlinear stability of a simplified model for the simulation of double suspension roofs. Eng Struct 2001;23:705–14.
[8] Raftoyiannis IG, Michaltsos GT. Nonlinear dynamic stability of multi-suspended roof systems. In: Proceedings of ICTAM'04, Warsaw (PL); 2004.
[9] Saafan AS. Theoretical analysis of suspension roofs. J Struct Div ASCE 1970;96(2):393–405.
[10] Kunieda H. Parametric resonance of suspension roofs in wind. J Eng Mech Div 1976;102(1):59–75.
[11] Scalzi JB. Cable-suspended roof construction. State-of-the-art. J Struct Div ASCE 1971;97(6):1715–61.
[12] Eurocode 1 (EC 1). Actions on structures. European Committee for Normalization CEN, Brussels; 1991.
[13] Naeim F. On seismic design implications of the 1994 Northridge earthquake records. Earthquake Spectra 1995;11(1):91–109.
[14] Manfredi G, Polese M, Cosenza E. Cumulative demand of the earthquake ground motions in the near source. J Earthquake Eng Struct Dyn 2003;32:1853–65.
[15] Hall JF. Near-source ground motion and its effects on flexible buildings. Earthquake Spectra 1995;11(4):569–605.
[16] Pavlou EA, Constantinou MC. Response of elastic and inelastic structures with damping systems to near-field and soft-soil ground motions. Eng Struct 2004;26:1217–30.
[17] Mavroeidis GP, Dong G, Papageorgiou AS. Near-fault ground motions and the response of elastic and inelastic single-degree-of-freedom (SDOF) systems. J Earthquake Engng Struct Dyn 2004;33:1023–49.
[18] Alavi B, Krawinkler H. Strengthening of moment-resisting frame structures against near-fault ground motion effects. J Earthquake Eng Struct Dyn 2004;33:707–22.
[19] Bertero VV, Mahin SA, Herrera RA. Aseismic design implications of San Fernando Earthquake Records. J Int Assoc Earthquake Eng 1978;6(1):31–42.
[20] Bolt BA. From earthquake acceleration to seismic displacements. The fifth Mallet-Milne lecture. New York: Wiley; 1996.
[21] Building Seismic Safety Council BSSC, NEHRP. Recommended provisions for seismic regulations for new buildings and other structures (FEMA 450); 2003 edition.
[22] International Building Code IBC 2000. International Code Council ICC, Whittier, CA; 2000.
[23] EAK, Greek Aseismic Code. OASP, Athens; 2000.
[24] Uniform Building Code UBC 1997. International Conference of Building Officials ICBO. Whittier, CA; 1997.
[25] Spyrakos CC, Maniatakis ChA, Taflambas J. Evaluation of near-field seismic records based on damage potential parameters – case study: Greece. Soil Dyn Earthquake Eng 2007. doi:10.1016/j.soildyn.2007.10.003.
[26] Bommer JJ, Georgallides G, Tromans IJ. Is there a near-field for small-to-moderate magnitude earthquakes? J Earthquake Eng 2001;5(3):395–423.
[27] Spyrakos CC, Maniatakis ChA, Taflambas J. Critical evaluation of near-source seismic records in Greece. In: Proceedings of ERES'05, Skiathos, Greece; 2005. p. 53–62.
[28] Spyrakos CC, Touliatos P, Patsilivas D, Pelekis G, Hampesis A, Maniatakis ChA. Seismic analysis and retrofit of a historic masonry building. In: Proceedings of ERES'05, Skiathos, Greece; 2005. p. 523–32.
[29] Chopra AK, Chintanapakdee C. Comparing response of SDOF systems to near-fault and far-fault earthquake motions in the context of spectral regions. J Earthquake Eng Struct Dyn 2001;30:1769–89.
[30] MacRae GA, Mattheis J. Three-dimensional steel building response to near-fault motions. J Struct Eng 2000;126(1):117–26.
[31] Fajfar P, Vidic T, Fischinger M. A measure of earthquake motion capacity to damage medium-period structures. J Soil Dyn Earthquake Eng 1990;9(5):236–42.
[32] Malhotra PK. Response of buildings to near-field pulse-like ground motions. J Earthquake Eng Struct Dyn 1999;28:1309–26.
[33] Iwan WD. Drift spectrum: measure of demand for earthquake ground motions. J Struct Eng ASCE 1997;123(4):397–404.
[34] Craig RR. Structural dynamics. New York: John Wiley & Sons; 1981.
[35] Davis PJ, Rabinowitz P. Methods of numerical integration. 2nd ed. New York: Academic Press; 1975.
[36] Wolfram S. Mathematica. 4th ed. UK: Cambridge University Press; 1999.
[37] Papazachos B, Papazachou C. The earthquakes in Greece. Thessaloniki: Ziti Publ.; 1997.
[38] Institute of Engineering Seismology and Earthquake Engineering ITSAK. Strong motion recordings of the ITSAK Network; 1980–1997.
[39] PEER Strong Motion Database. <http:/www.peer.berkeley.edu>.
[40] Jaramillo ABA. Seismological criteria for selecting and scaling real accelerograms for use in engineering analysis and design. Master Dissertation. Rose School, European School of Advanced Studies in Reduction of Seismic Risk; 2003.